Nuclear Instruments and Methods in Physics Research A 610 (2009) 644–648

Contents lists available at ScienceDirect

Nuclear Instruments and Methods in Physics Research A

journal homepage: www.elsevier.com/locate/nima

TwinGrid: A wafer post-processed multistage Micro Patterned Gaseous Detector

Y. Bilevych [a], V.M. Blanco Carballo [b,*], M. Chefdeville [a], M. Fransen [a], H. van der Graaf [a], C. Salm [b], J. Schmitz [b], J. Timmermans [a]

[a] Nikhef, Science Park 105, 1098 XG Amsterdam ,The Netherlands
[b] University of Twente/MESA+ Institute for Nanotechnology, Hogekamp 3214, PO Box 217, 7500 AE Enschede, The Netherlands

ARTICLE INFO

Article history:
Received 22 August 2009
Received in revised form
4 September 2009
Accepted 19 September 2009
Available online 26 September 2009

Keywords:
GEM
Micromegas
MPGD
SU-8
CMOS post-processing
Above-IC
Microsystems
Radiation detectors
Proportional chambers

ABSTRACT

This paper presents a new multistage Micro Patterned Gaseous Detector (MPGD) made by wafer post-processing. The device consists of a double metal grid supported by SU-8 structures on top of a Timepix chip. The detector has been operated with He/iC_4H_{10} and Ar/iC_4H_{10} gas mixtures. Cosmic rays as well as ^{55}Fe decay events have been recorded using the Timepix chip in 2D and 3D readout modes. The detector can be operated like a Micromegas (high field close to the chip) or like a GEM (amplification stage followed by a low extraction field). This approach for manufacturing GEM-like radiation imaging detectors allows for precise dimensional control and considerable geometrical design freedom.

1. Introduction

The use of multistage gaseous radiation detectors has been widely reported. Since the invention of the GEM detector [1,2], other devices like PIM [3], Micromegem [4], GEM-MIGAS [5], and especially, double or triple GEM configurations have been successfully operated. The multistage configuration can combine high gain with a low risk of discharges [6]. For instance, a triple GEM stack coupled to a Timepix chip [7] has been operated without sparking damage, reaching high enough gain for minimum ionizing particle detection [8].

Manually assembled multistage detectors suffer from misalignment between the GEM holes and the underlying chip pixels. Fabricating punctured metal foils directly on a chip, or wafer, using photolithography solves this problem. Fully functional detectors were recently shown using this fabrication approach, both Micromegas-like (Ref. [9], and references therein) and GEM-like [10]. The two differ in the amount of insulating material supporting the grid plane: either it is minimized (leading to sparse pillars, a geometry similar to Micromegas [11]) or instead it is maximized, only leaving openings where the gas avalanches occur (similar to GEM foils).

In this paper we show results obtained with the first multistage detectors integrated on top of CMOS chips using wafer post-processing techniques. We report on the fabrication process, energy resolution, gain, and imaging of X-ray and cosmic radiation.

2. Detector fabrication

In previous work SU-8 photoresist has been used as insulating support material to fix the position of punctured electrodes [9,10]. SU-8 has also been applied in microsystem technology to produce multilayer structures, typically by spin-coating and exposing several stacked SU-8 films, followed by a single development step [12–14]. We therefore employ SU-8 in a similar fashion to realize multistage MPGDs.

One important consideration when producing the multilayer structure is its mechanical robustness. Fig. 1 shows a prototype with two electrode planes over a Timepix microchip. The lower electrode is supported by a thick film of SU-8, only perforated under the electrode openings. The upper electrode is sparsely supported by pillars. Such a structure can be produced by simply

* Corresponding author. Tel.: +31 53 489 2648; fax: +31 53 489 1034.
E-mail address: C.Salm@utwente.nl (C. Salm).

0168-9002/$ - see front matter © 2009 Elsevier B.V. All rights reserved.
doi:10.1016/j.nima.2009.09.054

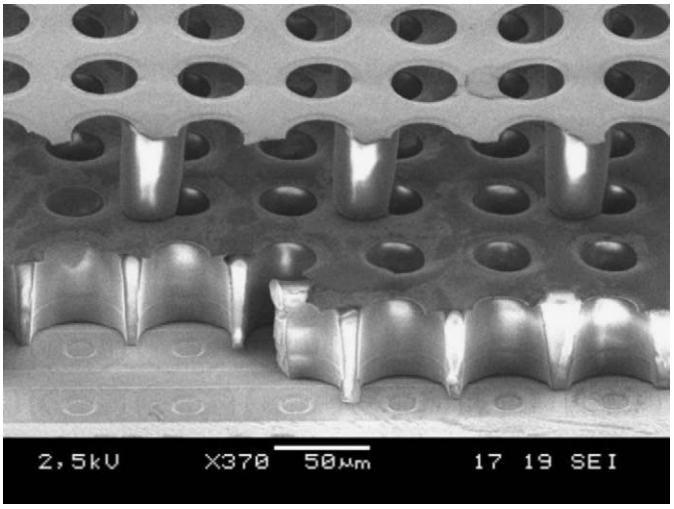

Fig. 1. SEM picture of a gas amplification structure on a Timepix chip. It comprises a lower stage with maximum amount of insulating material (for maximum support) and an upper stage with minimum insulating material (pillars).

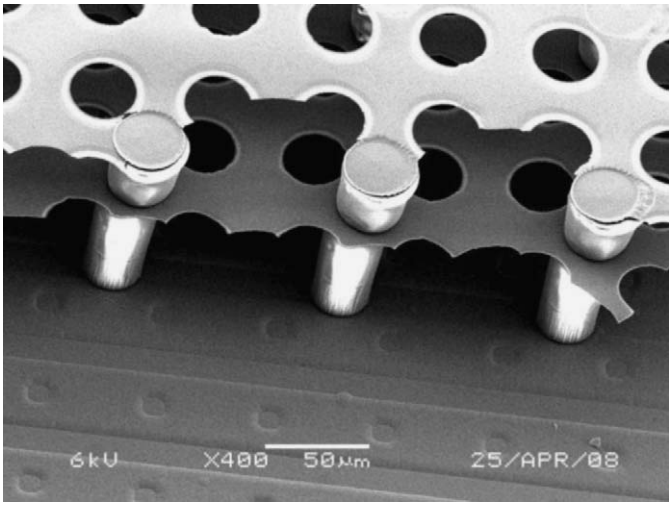

Fig. 2. SEM picture of a sparsely supported dual-stage gas amplification structure on a Timepix chip. The lower layer (pillars+electrode) was fabricated with the traditional process [6]; the upper layer was made using SU-8 foils.

repeating the standard fabrication procedure for single grids as documented in Ref. [9]. The structure is opened up in a single SU-8 development step, releasing the upper electrode and opening the holes in the bottom grid. The bottom layer is strong enough to survive the top-grid processing steps.

On the contrary, when the bottom layer is sparsely supported we found that the normal use of liquid SU-8 for the upper part leads to deformation on the lower part. The structure is thus destroyed before its production is finished. The deformation takes place while curing the spin-coated liquid SU-8 at a temperature above 35 °C. The lower SU-8 layer apparently reflows during this step. To overcome this problem, we switched to a less established, new approach. The upper SU-8 is not spin-coated and baked; instead, solid SU-8 films are laminated over the bottom grid. As the material is solid from the start, neither spinning nor curing is needed.

We deposit SU-8 foils on the underlying substrate by the following three steps:

- Lamination of two 20 µm thick SU-8 foils in a hot roller laminator at 70 °C, one after another.
- Masked exposure of the resist to define the pillars (400 mJ/cm^2 near UV broad band 350–450 nm).
- Overnight post-exposure bake of the resist at room temperature.

The 20-µm foil is the thickest one obtained from the supplier Microchem. Using this alternative procedure for the top layer, we have successfully manufactured a dual-stage gas amplification structure with sparse support pillars for both levels. A bird's eye SEM photograph of such a structure is shown in Fig. 2. For structures as shown in Figs. 1 and 2, manufactured by wafer post-processing, we use the term "TwinGrid" as an abbreviation of twin-integrated grid.

3. TwinGrid gain and energy resolution

The gain and energy resolution of TwinGrid detectors were studied using structures built on dummy silicon substrates with an aluminized anode. The measurements shown in this section were carried out on a TwinGrid as depicted in Fig. 1.

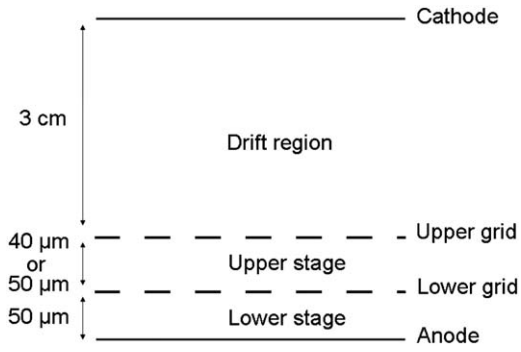

Fig. 3. Schematic picture of the different electrodes and stages in a TwinGrid detector.

The samples were tested inside a chamber consisting of an aluminum base plate covered with a Kapton gas seal. The gas (Ar/iC_4H_{10} (95/5)) was flushed through the chamber using feed-throughs in the seal cover. The induced signals at the anode are amplified using a charge-sensitive amplifier, connected to a multi-channel-analyzer from Amptek. Fig. 3 presents a schematic of the different electrodes and stages in a TwinGrid detector, also defining the detector's drift region and avalanche stages. In these studies the anode plane was always at ground potential.

At first, the device was operated in what we call the GEM mode: a high (multiplication) field in the upper stage, and a low (extraction) field in the lower stage. To achieve this, the lower grid was kept at a constant value of −50 V and the upper grid voltage was increased while maintaining the drift field constant. In this configuration electron multiplication takes place in the upper stage. In this GEM-mode we assume that sparks are least likely to damage the chip, as the field strength close to the chip is low.

A typical ^{55}Fe spectrum as recorded by the multi-channel-analyzer is shown in Fig. 4. Fig. 5 shows the gain curve and the energy resolution measured with TwinGrid as derived from such spectra. A gain of several thousands and an energy resolution better than 20% FWHM was achieved. Remarkably this GEM-like operation exhibits similar gain and energy resolution as Micromegas-like measurements, where the gain mainly takes place in the lower stage. This is in contrast to earlier reports on GEM and Micromegas [15,16], where the GEM resolution is usually found to

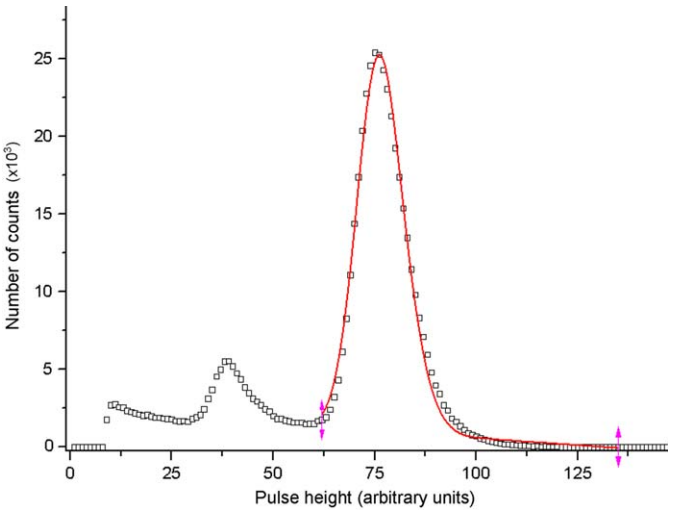

Fig. 4. Typical ^{55}Fe spectrum displayed by the multi-channel-analyzer obtained with a TwinGrid device operated in an Ar/iC$_4$H$_{10}$ (95/5) gas mixture. The main peak of the spectrum is fitted to a double Gaussian over a linear background function, using the least-squares method.

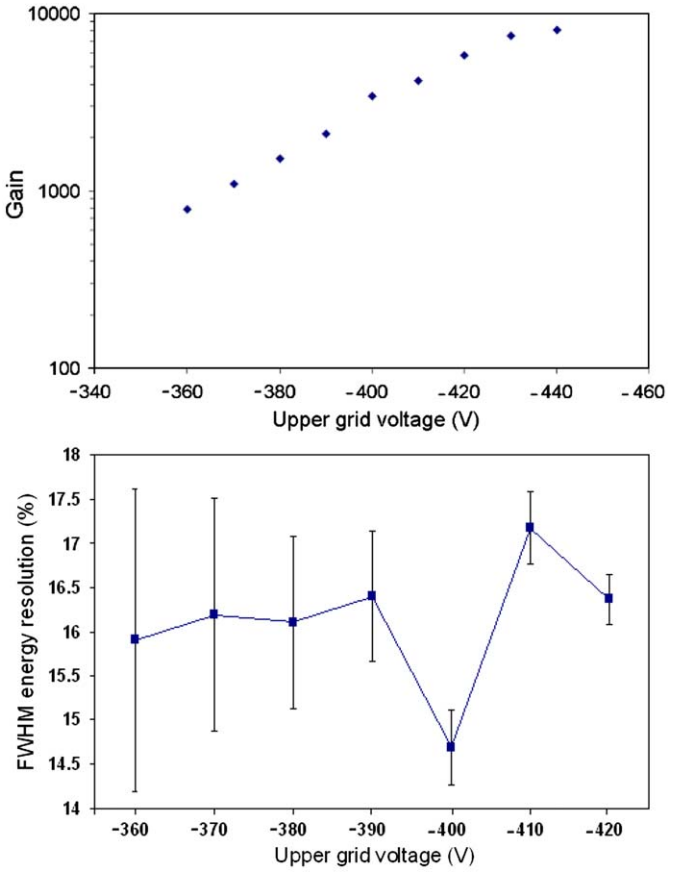

Fig. 5. TwinGrid gas gain (top) and ^{55}Fe energy resolution (bottom) in Ar/iC$_4$H$_{10}$ (95/5). The drift field is kept at 1.2 kV/cm and −50 V is applied to the lower grid. The values are extracted from the fitting as shown in Fig. 4. The error bars account for the estimated error on the multichannel-analyzer calibration. The statistical errors are negligible.

be worse than the one of Micromegas. We conclude that the reported performance of a single GEM can still be improved. The good control of dimensions in our manufacturing approach may be the root cause for the better performance. In addition to the good dimensional control, the extraction efficiency in our

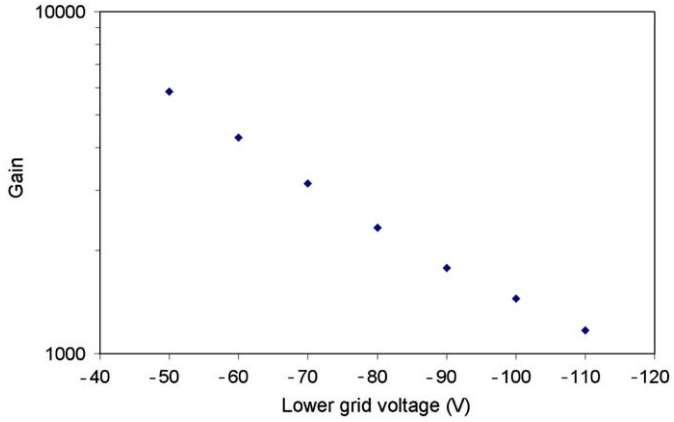

Fig. 6. TwinGrid gain curve in Ar/iC$_4$H$_{10}$ (95/5). The drift field is kept at 1.2 kV/cm and −420 V is applied to the upper grid.

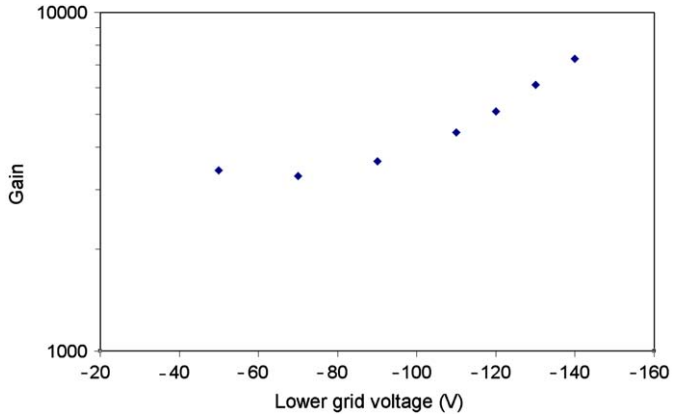

Fig. 7. TwinGrid gain curve in Ar/iC$_4$H$_{10}$ (95/5). The drift field is kept at 1.2 kV/cm and the upper stage field is kept at 70 kV/cm. The increasing gain indicates that multiplication occurs in the lower stage.

experiments is probably better than in a standard GEM as the extraction field is stronger.

More measurements were done to confirm the correct behavior of the device. The upper grid voltage and the drift field were kept constant while the lower grid voltage was increased. As expected in the GEM mode, lowering the field in the upper stage decreases the gain (see Fig. 6).

The gain of the device can thus be distributed between upper stage and lower stage. To test this, the device was operated with a constant 70 kV/cm field in the upper stage, and the drift field kept at 1.2 kV/cm. The lower grid voltage was varied. Fig. 7 shows the obtained gain curve. The total gain of the device remains constant until a certain lower grid voltage (around −80 V) when amplification in the lower stage starts to occur. At this voltage the total gain of the device is the product of the upper stage gain (kept at a constant value) and the lower stage gain (being varied). A high overall gain can thus be achieved with a relatively small gain in the lower stage.

4. Experience with sparking

The TwinGrid structure was originally conceived as a possible solution to the sparking problem observed in this kind of microsystems. Sudden death occurs on chips operating in gaseous radiation detectors, whether we use Micromegas or Ingrid electrode planes. In some cases, chips fail after only a few hours

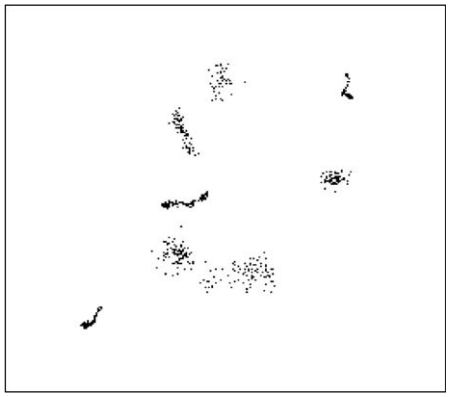

Fig. 8. Image of eight ^{55}Fe clouds in He/iC$_4$H$_{10}$ (77/23) spread over the chip area recorded with a 3 cm drift gap chamber. The chip area is approximately 14 mm × 14 mm.

of normal operation. The present solution to this sparking problem is to cover the chip surface with a high-ohmic layer of a few micrometers thickness. With a multistage detector, the multiplication field can be moved away from the chip surface. Sparks are then less likely to damage the chip. This could be an alternative solution to the sparking problem.

A Timepix chip without any spark protection layer was equipped with a TwinGrid structure as depicted in Fig. 2 and irradiated with an ^{55}Fe source. A He/iC$_4$H$_{10}$ (77/23) gas mixture was used to minimize the risk of sparks. The device was biased applying −450 and −130 V to the upper grid and lower grid, respectively. The electric field facing the chip was thus reduced from typically 100 kV/cm in the normal InGrid to 30 kV/cm in the TwinGrid. An even lower field at the chip surface should be feasible at acceptable detector performance.

The detector initially performed well. Fig. 8 shows several ^{55}Fe decay events obtained in this configuration using a 3 cm drift gap field cage (see Ref. [9] for details on how to interpret this image). However, after 5 h of operation the chip ceased to respond. This sudden death was comparable to earlier findings with chips not covered with a spark protection layer.

Further tests, especially using very low fields in the lower stage, are necessary to investigate if the TwinGrid detector can be operated in a spark-proof mode. At this point (after observing a case of sudden death) we can only conclude that the TwinGrid geometry is not the definitive solution against sparks.

5. Imaging with TwinGrid on a Timepix chip

After the experience described in Section 4, we switched back to a high-resistive protection layer on the readout chip. TwinGrid structures as depicted in Fig. 1 were fabricated on top of Timepix chips covered with a spark-protection layer of 11 μm silicon-rich silicon nitride. For 2-D and 3-D radiation imaging, the chip was wire bonded on a printed circuit board. The region around the chip was sealed by a field cage, that formed a 3 cm drift gap defined by the chip and a Kapton cathode plane. The chip was controlled and read out through a MUROS interface [17] using Pixelman software [18]. More details about the test chamber can be found in Ref. [9].

We observed ^{55}Fe events, tracks from cosmic rays, and tracks of electrons emitted by a ^{90}Sr source when operating the device at −200 V on the lower grid and −620 V on the upper grid using a He/iC$_4$H$_{10}$ (77/23) gas mixture. Cosmic rays were also detected when applying −100 V on the lower grid and −540 V on the upper grid. Two typical examples of cosmic tracks are shown in Fig. 9. The single-electron efficiency was not determined from these recorded data; however, assuming an exponential gain distribution and a pixel threshold of 1000 electrons a single electron efficiency of 90% is expected when −440 and −50 V are applied to upper grid and lower grid, respectively [19].

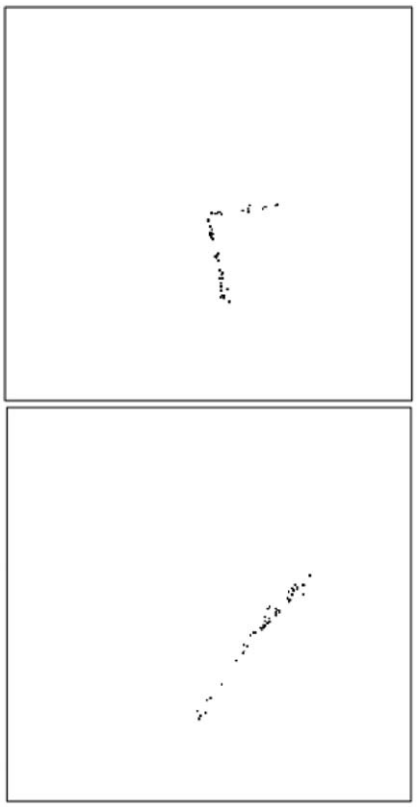

Fig. 9. Two events produced by cosmic rays crossing the detector area.

These imaging results are hardly distinguishable from earlier images obtained with an Ingrid-covered Timepix chip. From a radiation imaging point of view, the devices work similarly whether one or two electrodes are stacked on the chip.

However, the multigrid structure does have special features that may allow better performing detectors in some applications. First, the ion backflow can probably be reduced to much lower fractions than with a single grid. For TPC purposes this extends the rate capability of the detector. Arrangements with multiple grids allow gating, to further reduce the ion poisoning in the drift region.

Second, the signal development on the anode is faster in a multigrid arrangement operated in GEM-like mode, than when the avalanche develops between the lowest grid and the anode plane [20,21]. As the gas avalanche (and thus the positive charge) is electrostatically screened from the readout plane by the bottom grid, one may expect that only fast-drifting electrons create a signal at the readout plane. Further work is underway to obtain quantitative results on ion feedback and signal development speed.

6. Outlook

The two TwinGrid structures shown in Figs. 1 and 2 are only examples of a wide variety of possible multigrid arrangements. With the two extreme support approaches of "sparse pillars" and "maximized dielectric support", two more TwinGrid varieties are feasible. Realizations of these two are shown in Fig. 10 (top and

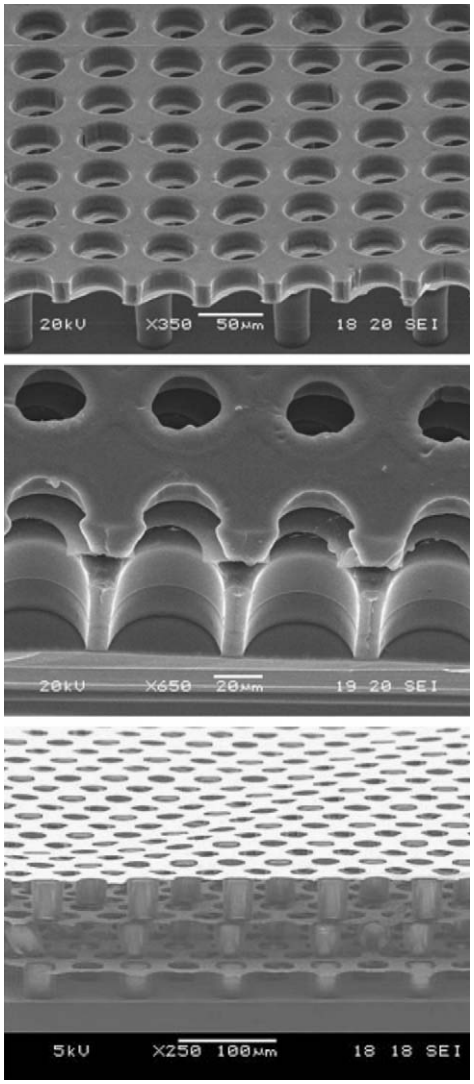

Fig. 10. Top: SEM picture of a GEMGrid on top of Ingrid. Middle: SEM picture of a GEMGrid on top of GEMGrid. In both cases the lower layer and upper layer are 50 and 20 μm thick, respectively. The upper grid is made with non-recessed SU-8. The upper metal electrode is 100 nm thick. Bottom: SEM picture of a triple grid structure.

middle). The fabrication is very similar; small differences in functionality may be expected but these are not yet investigated. The upper layer was made with a single (20-μm) SU-8 foil, just to illustrate the capability.

A three-layer stack can be produced following the same fabrication process employed for the TwinGrid devices. Fig. 10 (bottom) shows a SEM picture of a so-called triple grid structure, fabricated with liquid-SU-8 only. Similar-geometry triple grids have also been successfully realized with SU-8 foils. Stacking can be further continued, at the expense of production complexity and (therefore) possible yield reduction.

The structures shown in Fig. 10 have not been tested under high voltage conditions and radiation. They are presented here to illustrate this technology's design freedom.

7. Conclusions

We have presented fabrication approaches for multi-stage radiation detectors using wafer post-processing. Using the resulting so-called TwinGrid devices, cosmic rays and X-rays from an ^{55}Fe source have been detected. A gain of several thousands is routinely achieved, leading to an ^{55}Fe energy resolution below 20% FWHM. A wide variety of multi-stage MPGDs can be fabricated in the proposed manner, allowing for a detailed optimization of detector gain, resolution, rate capability, ion backflow, and signal speed.

Acknowledgements

This research is funded by the Dutch Foundation for Fundamental Research on Matter (FOM) and by the Dutch Technology Foundation STW through project TET 6630 "Plenty of room at the top". The authors would like to thank Bijoy Rajasekharan, Joost Melai and Jiwu Lu for the cleanroom help, Sander M. Smits for mask design and Joop Rövekamp for the mechanical support.

References

[1] F. Sauli, Nucl. Instr. and Meth. A 386 (2–3) (1997) 531.
[2] C. Büttner, M. Capeáns, W. Dominik, M. Hoch, J.C. Labbé, G. Manzin, G. Million, L. Ropelewski, F. Sauli, A. Sharma, Nucl. Instr. and Meth. A 409 (1–3) (1998) 79.
[3] D. Thers, T. Bretonniere, G. Charpak, P. Coulon, P. Leray, C. Drancourt, M. Le Guay, S. Lupone, L. Luquin, G. Martínez, M. Meynadier, P. Pichot, Nucl. Instr. and Meth. A 504 (1–3) (2003) 161.
[4] O. Bouhali, G. De Lentdecker, S. Dewèze, F. Udo, W. Van Doninck, C. Vander Velde, L. Van Lancker, V. Zhukov, I. Boulogne, E. Daubie, Nucl. Instr. and Meth. A 459 (1–2) (2001) 211.
[5] J.A. Mir, R. Stephenson, N.J. Rhodes, E.M. Schooneveld, J.F.C.A. Veloso, J.M.F. Dos Santos, Nucl. Instr. and Meth. A 573 (1–2) (2007) 179.
[6] S. Bachmann, A. Bressan, M. Capeáns, M. Deutel, S. Kappler, B. Ketzer, A. Polouektov, L. Ropelewski, F. Sauli, E. Schulte, L. Shekhtman, A. Sokolov, Nucl. Instr. and Meth. A 479 (2–3) (2002) 294.
[7] X. Llopart, R. Ballabriga, M. Campbell, L. Tlustos, W. Wong, Nucl. Instr and Meth. A 581 (1–2) (2007) 485;
Erratum Nucl. Instr. and Meth. A 585 (1–2) (2008) 106–108.
[8] A. Bamberger, K. Desch, U. Renz, M. Titov, N. Vlasov, P. Wienemann, A. Zwerger, Nucl. Instr. and Meth. A 573 (3) (2007) 361.
[9] V.M. Blanco Carballo, M. Chefdeville, M. Fransen, H. van der Graaf, J. Melai, C. Salm, J. Schmitz, J. Timmermans, IEEE Electron Devices Lett. 29 (6) (2008) 585.
[10] V.M. Blanco Carballo, Y. Bilevych, M. Chefdeville, M. Fransen, H. van der Graaf, C. Salm, J. Schmitz, J. Timmermans, Nucl. Instr. and Meth. A 608 (1) (2009) 86.
[11] Y. Giomataris, Ph. Rebourgeard, J.P. Robert, G. Charpak, Nucl. Instr. and Meth. A 376 (1) (1996) 29.
[12] F. Ceyssens, R. Puers, J. Micromech. Microeng. 16 (6) (2006) S19.
[13] D. Sameoto, See-Ho Tsang, M. Parameswaran, Sensors and Actuators A 134 (2) (2007) 457.
[14] L.J. Guerin, M. Bossel, M. Demierre, S. Calmes, P. Renaud, in: TRANSDUCERS '97, the 9th International Conference on Solid State Sensors, Actuators and Microsystems, Chicago, IL, USA, June 16–19, 1997, pp. 1419–1422.
[15] A. Delbart, R. De Oliveira, J. Derré, Y. Giomataris, F. Jeanneau, Y. Papadopoulos, Ph. Rebourgeard, Nucl. Instr. and Meth. A 461 (1–3) (2001) 84.
[16] R. Bellazzini, A. Brez, G. Gariano, L. Latronico, N. Lumb, G. Spandre, M.M. Massai, R. Raffo, M.A. Spezziga, Nucl. Instr. and Meth. A 419 (2–3) (1998) 429.
[17] D. San Segundo Bello, M. van Beuzekom, P. Jansweijer, H. Verkooijen, J. Visschers, Nucl. Instr. and Meth. A 509 (1–3) (2003) 164.
[18] T. Holy, J. Jakubek, S. Pospisil, J. Uher, D. Vavrik, Z. Vykydal, Nucl. Instr. and Meth. A 563 (1) (2006) 254.
[19] M. Chefdeville, Ph.D. Thesis, University of Amsterdam, 2009.
[20] C.W. Fabjan, W. Riegler, Nucl. Instr. and Meth. A 535 (1–2) (2004) 79.
[21] S. Bachmann, A. Bressan, L. Ropelewski, F. Sauli, A. Sharma, D. Mörmann, Nucl. Instr. and Meth. A 438 (2–3) (1999) 376.